
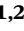



# A dual center and dual vendor comparison study of automated perfusion-weighted phase-resolved functional lung magnetic resonance imaging with dynamic contrast-enhanced magnetic resonance imaging in patients with cystic fibrosis

Lea Behrendt<sup>1,2</sup>  | Laurie J. Smith<sup>3</sup> | Andreas Voskrebenezv<sup>1,2</sup> | Filip Klimes<sup>1,2</sup>  | Till F. Kaireit<sup>1,2</sup> | Gesa H. Pöhler<sup>1,2</sup> | Agilo L. Kern<sup>1,2</sup>  | Cristian Crisosto Gonzalez<sup>1,2</sup> | Anna-Maria Dittrich<sup>2,4</sup> | Helen Marshall<sup>3</sup> | Katharina Schütz<sup>4</sup> | Paul J. C. Hughes<sup>3</sup> | Pierluigi Ciet<sup>5</sup> | Harm A. W. M. Tiddens<sup>5,6</sup> | Jim M. Wild<sup>3</sup> | Jens Vogel-Claussen<sup>1,2</sup>

<sup>1</sup>Department for Diagnostic and Interventional Radiology, Hannover Medical School, Hannover, Germany

<sup>2</sup>Biomedical Research in Endstage and Obstructive Lung Disease Hannover (BREATH), German Center for Lung Research (DZL), Hannover, Germany

<sup>3</sup>Department of Infection, Immunity and Cardiovascular Disease, POLARIS, Imaging Sciences, University of Sheffield, Sheffield, UK

<sup>4</sup>Department for Pediatric Pulmonology, Allergology and Neonatology, Hannover Medical School, Hannover, Germany

<sup>5</sup>Department of Pediatric Pulmonology and Allergology, Sophia Children's Hospital, Erasmus MC, Rotterdam, The Netherlands

<sup>6</sup>Department of Radiology and Nuclear medicine, Erasmus MC, Rotterdam, The Netherlands

## Correspondence

Jens Vogel-Claussen, Department for Diagnostic and Interventional Radiology, Hannover Medical School, Carl-Neuberg-Str. 1, Hannover 30625, Germany.  
Email: vogel-claussen.jens@mh-hannover.de

## Funding information

German Center for Lung Research (DZL); Cystic Fibrosis Foundation (CFF), Grant/Award Number: TIDDEN17A0

## Abstract

For sensitive diagnosis and monitoring of pulmonary disease, ionizing radiation-free imaging methods are of great importance. A noncontrast and free-breathing proton magnetic resonance imaging (MRI) technique for assessment of pulmonary perfusion is phase-resolved functional lung (PREFUL) MRI. Since there is no validation of PREFUL MRI across different centers and scanners, the purpose of this study was to compare perfusion-weighted PREFUL MRI with the well-established dynamic contrast-enhanced (DCE) MRI across two centers on scanners from two different vendors. Sixteen patients with cystic fibrosis (CF) (Center 1: 10 patients; Center 2: 6 patients) underwent PREFUL and DCE MRI at 1.5T in the same imaging session. Normalized perfusion-weighted values and perfusion defect percentage (QDP) values were calculated for the whole lung and three central slices (dorsal, central, ventral of the carina). Obtained parameters were compared using Pearson correlation, Spearman correlation, Bland–Altman

This is an open access article under the terms of the Creative Commons Attribution-NonCommercial License, which permits use, distribution and reproduction in any medium, provided the original work is properly cited and is not used for commercial purposes.

© 2022 The Authors. *Pulmonary Circulation* published by John Wiley & Sons Ltd on behalf of Pulmonary Vascular Research Institute.

analysis, Wilcoxon signed-rank test, and Wilcoxon rank-sum test. Moderate-to-strong correlations between normalized perfusion-weighted PREFUL and DCE values were found (posterior slice:  $r = 0.69$ ,  $p < 0.01$ ). Spatial overlap of PREFUL and DCE QDP maps showed an agreement of 79.4% for the whole lung. Further, spatial overlap values of Center 1 were not significantly different to those of Center 2 for the three central slices ( $p > 0.07$ ). The feasibility of PREFUL MRI across two different centers and two different vendors was shown in patients with CF and obtained results were in agreement with DCE MRI.

#### KEYWORDS

Fourier decomposition, free-breathing proton MRI, pulmonary MRI

## INTRODUCTION

Cystic fibrosis (CF) is a common progressive disease among Caucasians.<sup>1-3</sup> Lung disease is the main cause of morbidity and mortality in patients with CF, but implementation of a newborn screening test has led to early diagnosis and life expectancy for patients with CF has increased in recent years.<sup>1,4-6</sup> Therefore, improvements in imaging methods for sensitive diagnosis and monitoring of pulmonary disease are of great importance. High-resolution computed tomography is the most widely used method to assess morphological changes in CF-related lung disease.<sup>7</sup> However, the use of high-resolution computed tomography for short-term follow-up as well as lifelong monitoring is accompanied by a cumulative radiation dose and related risks.<sup>8,9</sup>

An ionizing radiation-free and established method to assess lung perfusion is dynamic contrast-enhanced (DCE) magnetic resonance imaging (MRI).<sup>10,11</sup> Although free-breathing DCE MRI techniques were shown in recent studies,<sup>12,13</sup> DCE MRI often requires a breath-hold for data acquisition and always the injection of gadolinium-based intravenous contrast agents, which are reported to cause side-effects in patients with renal failure and gadolinium deposition in different parts of the body.<sup>14-17</sup> This is a matter of concern, especially in children, where the long-term effect of gadolinium deposition in the brain is still unknown.<sup>18</sup>

Further, the required breath-hold maneuver might be impractical, especially in newborns, children, or patients with severe lung disease. Loss of breath-hold during acquisition could lead to image artifacts particularly in the region of the diaphragm due to respiratory motion.

With these issues in mind, validation of patient-friendly free-breathing contrast agent-free proton MRI techniques based on Fourier decomposition,<sup>19</sup> which allows for simultaneous assessment of lung ventilation and perfusion, is desirable. Since no ionizing radiation or contrast agent is

used, these techniques can be useful for long-term monitoring of children and adults with chronic lung diseases.<sup>20,21</sup>

The basic principle of Fourier decomposition is the registration of dynamic images, followed by Fourier transformation of the signal time series on a voxel level, allowing for distinct analysis of the respiratory and cardiac frequency components.<sup>19</sup> Phase-resolved functional lung (PREFUL) MRI extends the conventional Fourier decomposition approach by including the reconstruction of a full respiratory and cardiac cycle to gain dynamic ventilation and perfusion information.<sup>22-24</sup> Recently, the repeatability of ventilation and perfusion parameters derived by PREFUL MRI was shown<sup>25</sup> and ventilation parameters derived by PREFUL MRI and hyperpolarized <sup>129</sup>Xe MRI were compared.<sup>26,27</sup> Further, PREFUL MRI was already validated with DCE MRI in patients with different lung diseases in single center and single MRI vendor studies.<sup>21,28,29</sup> However, no feasibility study of PREFUL MRI across multiple centers utilizing different scanner vendors has yet been conducted.

Thus, the purpose of this dual center study was to compare perfusion-weighted PREFUL MRI across two different sites and two different scanners using a semi-quantitative approach with DCE MRI used as an established reference standard in patients with CF with a range of ages and lung disease severity. In advance, some modifications and improvements were made to the recently described PREFUL algorithm,<sup>29</sup> especially to the automated perfusion phase sorting algorithm. These modifications will be described in detail in the method section.

## METHODS

### Patient characteristics

A total of 16 patients with CF (Center 1: 10 patients, age range 12–18 years, 8 females; Center 2: 6 patients, age

range 19–47 years, 3 females) were included in this study. Inclusion criteria were a confirmed diagnosis of CF and an age in the range 12–60 years. Exclusion criteria were an incomplete MRI protocol and contraindications to MRI (e.g., claustrophobia, pregnancy, or pacemaker) and MRI contrast agent. Further exclusion criteria were recent (<1 month) respiratory tract exacerbation with use of intravenous antibiotics, chronic oxygen therapy, and any other severe comorbidities that could limit imaging. Demographic and clinical characteristics for all patients are given in Table S1.

## MRI scanning and data analyses

All scans were performed on 1.5T scanners, with free-breathing PREFUL MRI performed before DCE MRI in the same imaging session in all cases:

- Center 1: Siemens Avanto (Siemens Healthineers) with a 6-channel body matrix coil.
- Center 2: Signa HDxt (GE Healthcare) with an 8-channel cardio-thoracic coil.

An overview of the PREFUL and DCE postprocessing is shown in Figure S1, with the same post-processing technique being applied across centers. The data analysis was performed centrally by one investigator using MATLAB (Matlab 2018b, MathWorks).

## PREFUL MRI

For PREFUL MRI, between five and eight coronal slices, covering the whole lung, were acquired for each patient. These slices included three central slices, located dorsal, central, and ventral of the carina (see Figure 3 for exemplary slice locations), which are further referred to as the posterior, tracheal, and anterior slice. Analysis was performed for the whole lung and the three central slices since these three slices were acquired for all patients.

For Center 1, a spoiled gradient-echo sequence with the following settings was used: field of view  $380 \times 380$ – $500 \times 500$  mm<sup>2</sup>, matrix size  $128 \times 128$  (interpolated to  $256 \times 256$ ), slice thickness 15mm, 0 or 5 mm gap between slices, echo time 0.82–0.88 ms, repetition time 3 ms, flip angle 5°, bandwidth 1500 Hz/px, generalized autocalibrating partially parallel acquisitions (GRAPPA)<sup>30</sup>  $R = 2$  with acquisition of 24 autocalibration lines, temporal resolution 190–192.5 ms. 250 images per slice were obtained.

For Center 2, a spoiled gradient-echo sequence with the following settings was used: field of view  $480 \times 480$  mm<sup>2</sup>,

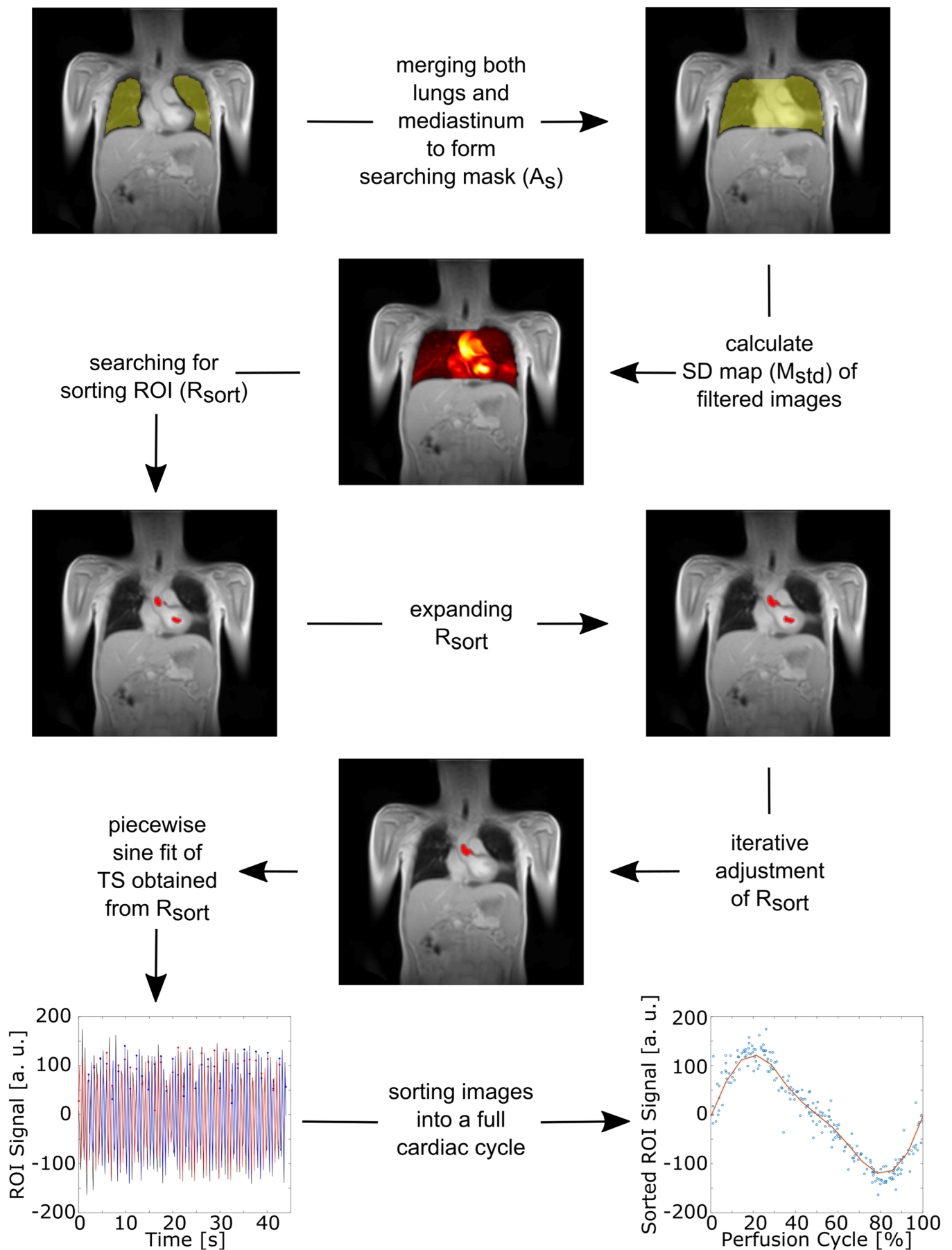
matrix size  $128 \times 128$  (interpolated to  $256 \times 256$ ), slice thickness 15 mm, 5 mm gap between slices, echo time 0.80 ms, repetition time 2.5 ms, flip angle 4°, bandwidth 1305 Hz/px, temporal resolution 373 ms. 250 images per slice were acquired.

Some modifications (including registration to end-inspiration and modification of the perfusion phase sorting algorithm [described further below]) were made to the recently described PREFUL postprocessing algorithm.<sup>29</sup> Since DCE data sets were acquired at end-inspiration, all PREFUL images were registered towards one fixed image at end-inspiration using the group-oriented registration approach.<sup>31</sup> For all registrations, the freely available Advanced Normalization Tools (ANTs<sup>32</sup>) were used. Segmentation of the lung boundaries was performed using a pre-trained convolutional neural network.<sup>33</sup> Then, images were automatically sorted according to their cardiac phase and interpolated to a full cardiac cycle (Figure 1). For this purpose, a modified version of the previously described automated sorting algorithm<sup>29</sup> was applied:

1. Both lungs and the mediastinum were included in a search region of interest (ROI) ( $A_s$ ).
2. A high-pass filter at 0.75 Hz<sup>29</sup> was applied to all registered images to remove signal variations caused by respiration. To get a simplified perfusion-weighted map ( $M_{std}$ ), the standard deviation of all images was computed for all voxels within  $A_s$ .
3. An ROI consisting of blood voxels ( $R_{sort}$ ) is needed to perform phase sorting. Therefore, all voxels above the 98<sup>th</sup> percentile of  $M_{std}$  were chosen for  $R_{sort}$ .
4. As a result,  $R_{sort}$  consisted of several voxel clusters.
5. To avoid clusters at the lung boundaries (especially at the diaphragm) being chosen for  $R_{sort}$ , due to remaining respiratory motion, all clusters connected to the boundaries of  $A_s$  were excluded.
6. A minimum of three voxels for each cluster was required. Therefore, each cluster was expanded as follows: A gradient map ( $M_{grad}$ ) of  $M_{std}$  was computed using the Sobel gradient operator. Since a high gradient difference between two adjacent voxels indicates a vessel boundary, an individual threshold ( $G_{lim}$ ) for each cluster defined by the mean plus standard deviation (SD) of  $M_{grad}$  inside each cluster was calculated as:

$$G_{lim} = \text{Mean}(M_{grad}(\text{cluster})) + (M_{grad}(\text{cluster})).$$

Then, for each cluster, the gradient values of all adjacent voxels were compared to  $G_{lim}$ . Voxels with values smaller than  $G_{lim}$  were included in the cluster.



**FIGURE 1** (See caption on next page)

7. Before the next step all but the 10 largest voxel clusters were removed from  $R_{\text{sort}}$ , to limit the processing time.
8. By performing a piecewise sinusoidal fit of the signal time series obtained by spatial averaging over  $R_{\text{sort}}$ , images were sorted according to their perfusion phase and interpolated to 15 phases at an equidistant time grid covering one cardiac cycle. To avoid different cardiac phases in the voxel clusters and to improve the sine fit,  $R_{\text{sort}}$  was iteratively adjusted by comparing the goodness of fit parameter  $R^2$  of the sinusoidal fit for all possible combinations of the voxel clusters. The cluster combination with the highest  $R^2$  value remained in  $R_{\text{sort}}$ .
9. Finally, images are sorted to their perfusion phase covering one cardiac cycle as described in Step 8 using the obtained  $R_{\text{sort}}$ .

Main vessels were excluded from the segmented lung parenchyma (Otsu's thresholding method<sup>34</sup>). Further, a perfusion-weighted PREFUL phase was selected as described previously.<sup>29</sup> First, for every voxel inside the lung parenchyma the phase of the reconstructed cardiac cycle with the maximal intensity was determined. Then, the most frequent phase was used as the perfusion-weighted PREFUL phase (Figure 2). For each study participant, perfusion-weighted PREFUL maps were normalized to the signal amplitude of  $R_{\text{sort}}$  of the individual's tracheal slice.

## DCE MRI

Both centers acquired DCE data in a single breath-hold at end-inspiration. A 3D time-resolved angiography with stochastic trajectories (TWISTs) sequence with the following settings was used by Center 1: field of view  $308 \times 380\text{--}406 \times 500 \text{ mm}^2$ , matrix size  $146 \times 256$  (interpolated to  $256 \times 256$ ), slice thickness 5 mm, echo time 0.80–0.86 ms, repetition time 2.4–2.5 ms, flip angle  $28^\circ$ , bandwidth 630 Hz/px, GRAPPA  $R = 4$ , temporal resolution 1.1–1.3 s.

Center 2 used a 3D gradient echo sequence with view sharing (TRICKS) with the following settings: field of view  $480 \times 480 \text{ mm}^2$ , matrix size  $120 \times 80$  (interpolated to

$256 \times 256$ ), slice thickness 10 mm, echo time 0.69 ms, repetition time 2.1 ms, flip angle  $30^\circ$ , bandwidth 2083 Hz/px, parallel imaging  $R = 2$ , temporal resolution 0.54–0.59 s.

For Center 1, a bolus of 0.03 mmol/kg bodyweight of gadoteric acid was injected at a rate of 4 ml/s. For Center 2, DCE MRI was acquired with injection of 0.05 mmol/kg bodyweight of gadobutrol at a rate of 4 ml/s.

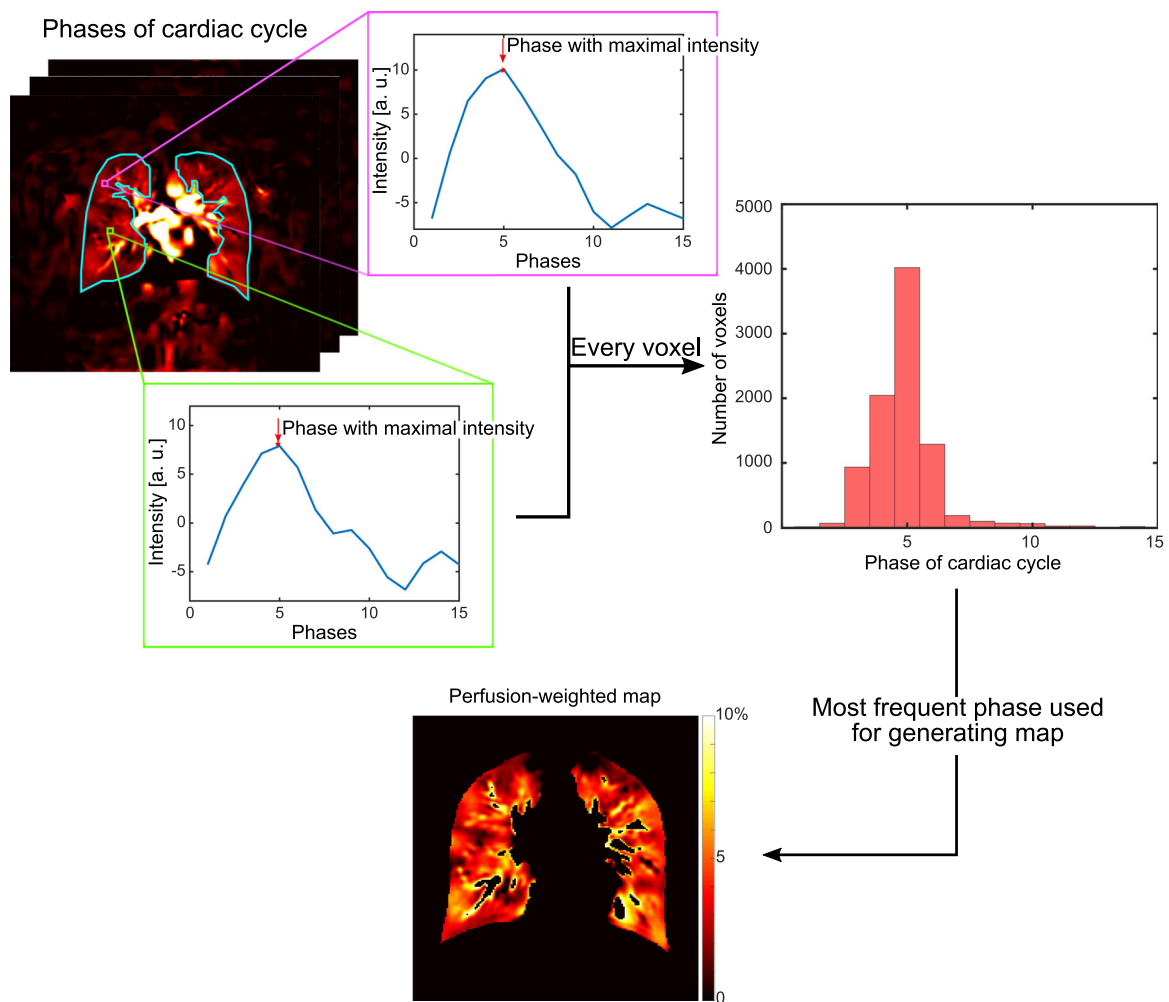
A perfusion-weighted phase of each DCE data set was selected as described recently.<sup>29</sup> First, an averaged signal time series over an ROI inside the aortic arch ( $R_{\text{aor}}$ ) on the coronal tracheal slice, showing the contrast agent intensity, was computed. The approach of placing an ROI inside the aortic arch for perfusion phase selection is similar to one used for perfusion assessment in computed tomography where an ROI is placed in the ascending aorta.<sup>35,36</sup> Then, a baseline was defined from all time points before the bolus arrival in the aorta. To ensure that the contrast agent has passed through the lung parenchyma, the first time point after baseline, which was located above the level of the second SD of the baseline, was selected as the perfusion-weighted DCE phase (Figure S2). Then, the perfusion-weighted DCE maps were filtered using a 3D Gaussian smoothing kernel with SD of 1 to reduce image noise. Finally, the perfusion-weighted DCE maps were normalized to the signal amplitude inside  $R_{\text{aor}}$ .

## Alignment of PREFUL and DCE

Due to thinner slice thickness of DCE MRI in comparison with PREFUL MRI, a compound coronal DCE slice corresponding to the PREFUL slice thickness and location was calculated as described recently.<sup>29</sup> First, DCE slices were multiplied by a normalized slice-overlap weighting factor. Afterward, the compound slice was obtained by summation over the weighted DCE slices. The normalized slice-overlap weighting factor is defined as the part of the width of the DCE slice overlapping the PREFUL slice divided by the slice thickness of the DCE slice.

For better comparison, PREFUL images, maps, and segmentation masks (including main vessels to avoid misalignment between previous excluded vessels from

**FIGURE 1** Automated phase-resolved functional lung (PREFUL) phase sorting and reconstruction of a full cardiac cycle. First, the lung boundaries were segmented using a convolutional neural network. Then, both lungs and the mediastinum are merged to form a searching mask ( $A_s$ ) for selection of the sorting region of interest (ROI). After expansion of the sorting ROI ( $R_{\text{sort}}$ ), which was determined from the standard deviation map ( $M_{\text{std}}$ ) of high-pass filtered original images,  $R_{\text{sort}}$  is adjusted in an iterative process. Further, a piecewise sinusoidal fit of the obtained signal time series (TS) from  $R_{\text{sort}}$  is performed and images are sorted into a full cardiac cycle.



**FIGURE 2** Selection of a perfusion-weighted phase-resolved functional lung (PREFUL) phase. First, for every voxel, the phase of the reconstructed cardiac cycle with maximal signal intensity was determined. The most frequent phase was then used as the perfusion-weighted PREFUL phase.

the mask and the actual position of the vessels after registration of the PREFUL map) were registered to DCE images using a combination of rigid and nonrigid transformation. As for the registration during PREFUL postprocessing, ANTs<sup>32</sup> was used for PREFUL to DCE registration. Afterward, the segmentation masks were adjusted to the PREFUL and DCE lungs by removing parts which are not covered by both PREFUL and DCE (Figure S3) and excluding main vessels (present in DCE and/or PREFUL image). The resulting parenchyma mask was the same for PREFUL and DCE and it was used for all further analysis.

## PREFUL and DCE analysis

Using the same lung parenchyma mask for both PREFUL and DCE analysis allowed for the same ROIs to be used (with the compound DCE slices being used). The ROIs

used were: the total lung parenchyma, the left and right lung, and the segmented lung parenchyma divided into quadrants.

Median normalized perfusion-weighted PREFUL and DCE values were computed. For further analysis, perfusion defect percentage (QDP) maps were calculated using a threshold of 2% for PREFUL and 1.75% for DCE. Values below these thresholds were identified as perfusion defect. These thresholds were determined by a threshold analysis described in the appendix.

## Statistical tests

Functional MRI parameters were assessed using non-parametric tests, with the significance level set to 0.05, as the Kolmogorov–Smirnov test for normality was negative for all. Unless noted otherwise, data are presented as median with 25<sup>th</sup> and 75<sup>th</sup> percentiles.

For median normalized perfusion-weighted PREFUL and DCE values, Pearson correlation coefficients were calculated. Further, voxelwise Spearman correlation was performed for the normalized perfusion-weighted PREFUL and DCE values of all patients for the whole lung using (a) the interpolated image matrix size of  $256 \times 256$  and (b) a matrix size of  $64 \times 64$  to reduce the influence of noise to the correlation.

To assess the agreement between PREFUL and DCE QDP maps for both centers combined, Bland–Altman analysis was performed. QDP values were further evaluated by calculating Pearson correlation coefficients and applying a paired two-sided Wilcoxon signed-rank test. In addition, the spatial overlap between PREFUL and DCE QDP maps was calculated for nondefect and defect areas separately as well as for both areas combined. The spatial overlap was defined as the percentage of voxels in the lung parenchyma labeled as perfusion defect or healthy tissue with both methods.

In addition, Spearman correlation coefficients were calculated between forced expiratory volume in 1 s (FEV1) predicted values and QDP values derived by PREFUL and DCE MRI for the whole lung.

For both centers separately, median PREFUL and DCE QDP values of all patients were calculated and compared using a paired two-sided Wilcoxon signed-rank test. Moreover, spatial overlap values were tested for significant difference across centers using a Wilcoxon rank-sum test.

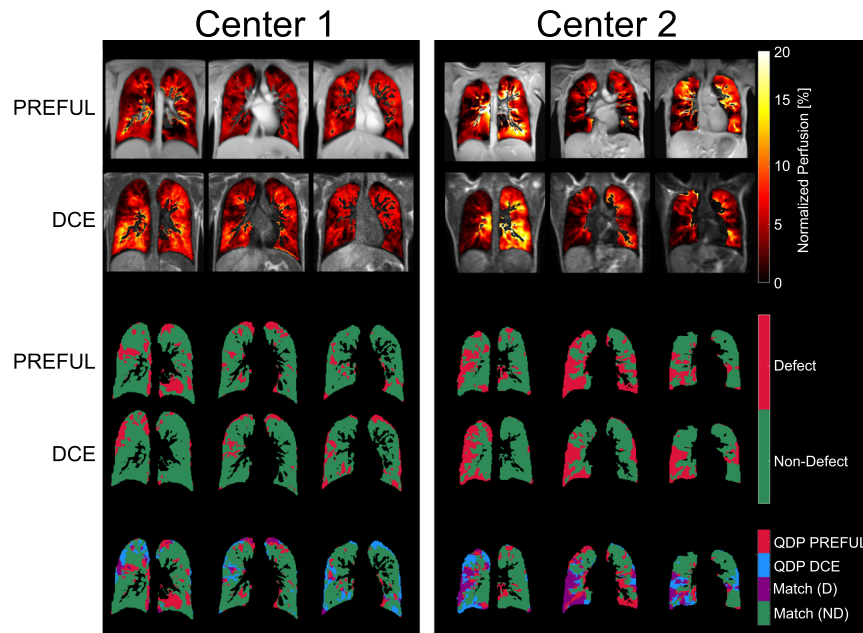
## RESULTS

One patient from Center 1 was excluded due to an incomplete MRI protocol (no DCE MRI).

Figure 3 shows exemplary PREFUL and DCE perfusion-weighted maps of the three central slices for one CF patient from each center along with the corresponding QDP maps and spatial overlap map.

### Normalized perfusion results

Significant moderate-to-strong Pearson correlations were seen between median normalized perfusion-weighted PREFUL and DCE values for some lung regions (Table 1). Voxelwise Spearman correlation coefficients



**FIGURE 3** Exemplary perfusion-weighted phase-resolved functional lung (PREFUL) (first row) and dynamic contrast-enhanced (DCE) (second row) maps, perfusion defect percentage (QDP) maps (third and fourth row), and maps showing the spatial overlap (fifth row) for the three central slices for a cystic fibrosis patient from each center (patient Center 1: 17 years old, female, FEV1 predicted 82.9%; patient Center 2: 19 years old, female, FEV1 predicted 32.7%). QDP values for the patient of Center 1 are 22.3%, 16.5%, and 9.1% (posterior to anterior) and 17.2% for the whole lung for PREFUL and 11.0%, 10.7%, and 18.4% (posterior to anterior) and 11.5% for the whole lung for DCE. For the patient of Center 2 the QDP values are 23.1%, 47.5%, and 22.5% (posterior to anterior) and 28.1% for the whole lung for PREFUL and 24.5%, 28.8%, and 29.2% (posterior to anterior) and 29.2% for the whole lung for DCE. FEV1: forced expiratory volume in 1 s. Match (D): QDP PREFUL/QDP DCE match of defect areas. Match (ND): QDP PREFUL/QDP DCE match of nondefect areas.

**TABLE 1** Pearson correlation coefficients of median normalized perfusion-weighted PREFUL and DCE values

ROI Slice	Total parenchyma		Right lung		Right upper lung		Right lower lung		Left lung		Left upper lung		Left lower lung	
	<i>r</i>	<i>p</i>	<i>r</i>	<i>p</i>	<i>r</i>	<i>p</i>	<i>r</i>	<i>p</i>	<i>r</i>	<i>p</i>	<i>r</i>	<i>p</i>	<i>r</i>	<i>p</i>
Whole lung	0.49	0.07	0.53	<b>0.04</b>	0.58	<b>0.02</b>	0.46	0.09	0.47	0.08	0.62	<b>0.01</b>	0.16	0.57
Posterior	0.69	<b>&lt;0.01</b>	0.75	<b>&lt;0.01</b>	0.82	<b>&lt;0.01</b>	0.56	<b>0.03</b>	0.47	0.08	0.78	<b>&lt;0.01</b>	0.02	0.95
Tracheal	0.45	0.09	0.44	0.10	0.56	<b>0.03</b>	0.34	0.22	0.46	0.08	0.59	<b>0.02</b>	0.09	0.75
Anterior	0.28	0.31	0.21	0.44	0.22	0.43	0.35	0.20	0.44	0.10	0.41	0.13	0.45	0.09

Note: Correlation coefficients calculated for Center 1 and Center 2 combined. Significant *p*-values are printed in bold.

Abbreviations: DCE, dynamic contrast-enhanced; PREFUL, phase-resolved functional lung; ROI, region of interest.

**TABLE 2** PREFUL and DCE QDP values and their spatial overlap for the whole lung and for the three central slices

	QDP[%]			Spatial overlap [%]		
	PREFUL	DCE	<i>p</i>	Nondefect area	Defect area	Combined areas
Whole lung	12.1 (7.6–18.6)	13.6 (4.6–28.4)	<b>0.89</b>	75.3 (60.8–89.0)	3.9 (0.7–8.3)	79.4 (69.2–89.4)
Posterior	13.8 (8.3–21.3)	11.0 (1.3–23.0)	<b>0.28</b>	79.7 (65.1–86.3)	1.4 (0.2–8.5)	83.6 (74.8–86.6)
Tracheal	16.5 (5.9–28.4)	10.8 (3.1–30.7)	<b>0.36</b>	74.3 (47.0–87.5)	2.7 (0.2–13.7)	76.9 (61.5–87.6)
Anterior	10.2 (4.3–21.5)	22.6 (7.0–31.5)	0.02	72.6 (61.8–88.6)	2.8 (0.1–10.8)	77.1 (70.4–88.6)

Note: Parameters calculated for Center 1 and Center 2 combined. The overlap is listed for the defected and nondefected lung regions as well as for both regions combined. *p*-values obtained by Wilcoxon signed-rank test. Nonsignificant *p*-values (no difference between QDP values) are printed in bold. Data presented as median with 25<sup>th</sup> and 75<sup>th</sup> percentiles in parentheses.

Abbreviations: DCE, dynamic contrast-enhanced; QDP, perfusion defect percentage; PREFUL, phase-resolved functional lung.

of 0.29 ( $p < 0.01$ ) for the  $256 \times 256$  matrix and 0.32 ( $p < 0.01$ ) for the  $64 \times 64$  matrix were found.

## QDP results

Median QDP values and spatial overlap values of all patients from both centers for PREFUL and DCE are presented in Tables 2 and S2. A median spatial overlap for DCE and PREFUL QDP maps of 79.4% was found for the whole lung. No significant differences in QDP values derived by PREFUL and DCE were observed for most lung regions for both centers combined. This was also seen in the Bland–Altman plots (Figure 4). However, a few patients showed large QDP differences ( $QDP_{DCE} - QDP_{PREFUL} > 10\%$ ). Exemplary PREFUL and DCE perfusion-weighted maps along with the corresponding QDP maps and spatial overlap map of two patients with large QDP differences are presented in Figure S4. Further, for most ROIs significant Pearson correlation coefficients between QDP values

derived by PREFUL on the one hand and DCE on the other hand were obtained (both centers combined, whole lung:  $r = 0.70$ ,  $p < 0.01$ ; Table 3).

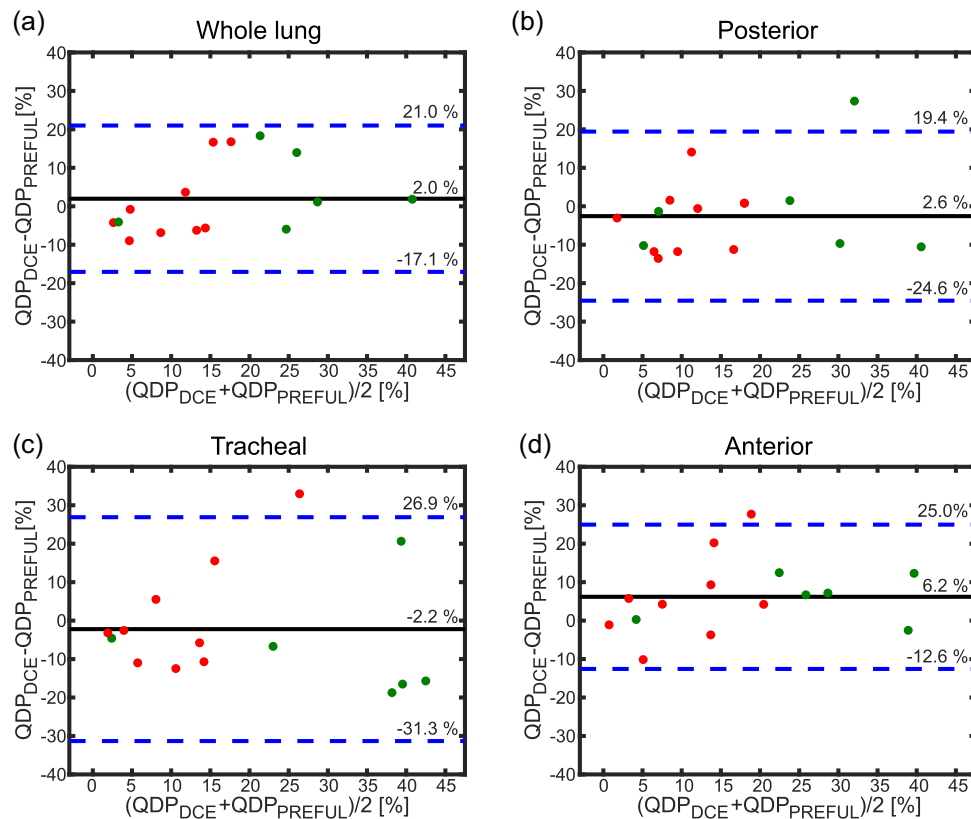
Spearman correlations for the whole lung between FEV1 predicted and QDP values derived by PREFUL ( $r = -0.61$ ,  $p = 0.02$ ) and DCE MRI ( $r = -0.49$ ,  $p = 0.06$ ) are shown in Figure S5 along with the linear regression lines.

For the whole lung, a median QDP of 10.1% (3.4%–16.2%) for DCE and of 9.3% (6.6%–13.2%) for PREFUL was obtained for Center 1 ( $p = 0.73$ ). In comparison, for Center 2, a median QDP of 29.9% (21.7%–33.0%) for DCE and of 23.4% (12.2%–28.1%) for PREFUL was found ( $p = 0.56$ ).

## Spatial overlap results

Figure 5 compares the spatial overlap values between PREFUL and DCE of Center 1 and Center 2. For the whole lung, a significant difference between spatial





**FIGURE 4** Bland–Altman plots comparing perfusion defect percentage (QDP) values of the cystic fibrosis patients derived by phase-resolved functional lung (PREFUL) and dynamic contrast-enhanced (DCE) magnetic resonance imaging obtained for both centers for the whole lung (a) and the three central slices (b–d). Values for Center 1 are marked in red and for Center 2 in green. Values of mean difference (black line) and mean difference  $\pm 1.96 \times$  standard deviation (blue dashed lines) are shown on right side of each plot.

overlap values of Center 1 and those of Center 2 was found ( $p = 0.03$ ) with median spatial overlap values of 84.7% (78.1%–90.9%) for Center 1 and of 68.6% (66.5%–69.7%) for Center 2. However, all three central slices showed no significant differences. For the posterior slice, the median spatial overlap values were 83.7% (78.8%–86.3%) and 70.6% (63.4%–86.8%) for Center 1 and Center 2 respectively ( $p = 0.27$ ). Further, median spatial overlap values of 82.8% (75.7%–89.5%) for Center 1 and of 62.0% (52.9%–75.4%) for Center 2 were obtained for the tracheal slice ( $p = 0.07$ ) and of 80.8% (76.2%–90.8%) (Center 1) and 70.5% (63.9%–74.7%) (Center 2) for the anterior slice ( $p = 0.07$ ).

## DISCUSSION

In this study, we compared PREFUL MRI with DCE MRI across two different sites and scanners from two different vendors in patients with CF.

DCE MRI is an established technique for assessment of lung perfusion and recent studies have found comparable

diagnostic accuracy of DCE MRI against planar scintigraphy and single-photon emission computed tomography (SPECT) ventilation/perfusion (V/Q) scans.<sup>10,11</sup> The design of our study did not include nuclear medicine Q scans, as SPECT or planar scintigraphy. Nevertheless, our previous single-center study showed that a specific phase of the reconstructed cardiac cycle of PREFUL MRI reflects pulmonary perfusion, as validated by SPECT Q scans. Further, in the same study, significant correlations were found between SPECT and DCE as well as between SPECT and PREFUL.<sup>29</sup> Therefore, a comparison between DCE and PREFUL should enable a reliable assessment. However, validation of PREFUL MRI with SPECT V/Q scans, as an overall accepted lung perfusion assessment tool, across different sites and scanners would be interesting, especially concerning the translation of PREFUL MRI to routine practice.

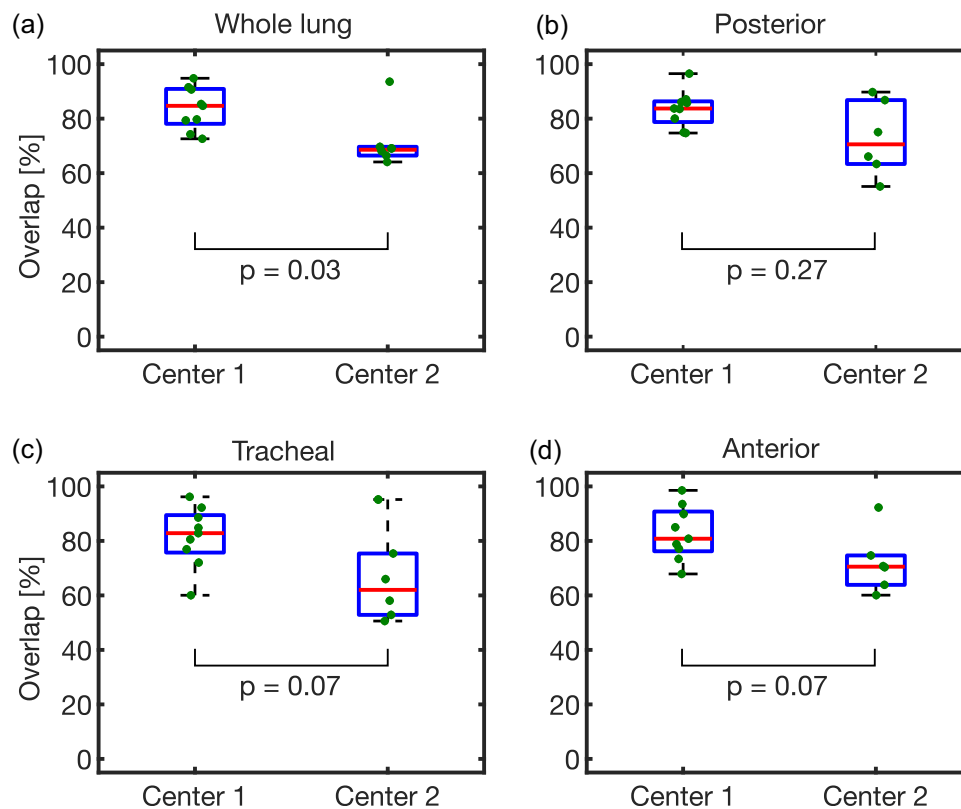
In accordance with recent single-center studies,<sup>29,37</sup> significant correlations (Pearson and Spearman) between perfusion-weighted PREFUL and DCE values were found. Voxelwise Spearman correlation was performed twice, with two different matrix sizes. The  $64 \times 64$  matrix

**TABLE 3** Pearson correlation coefficients of QDP values derived by PREFUL and DCE

ROI Slice	Total parenchyma		Right lung		Right upper lung		Right lower lung		Left lung		Left upper lung		Left lower lung	
	<i>r</i>	<i>p</i>	<i>r</i>	<i>p</i>	<i>r</i>	<i>p</i>	<i>r</i>	<i>p</i>	<i>r</i>	<i>p</i>	<i>r</i>	<i>p</i>	<i>r</i>	<i>p</i>
Whole lung	0.70	<b>&lt;0.01</b>	0.81	<b>&lt;0.01</b>	0.84	<b>&lt;0.01</b>	0.75	<b>&lt;0.01</b>	0.53	<b>0.04</b>	0.54	<b>0.04</b>	0.35	0.19
Posterior	0.62	<b>0.01</b>	0.73	<b>&lt;0.01</b>	0.82	<b>&lt;0.01</b>	0.46	0.09	0.45	0.09	0.46	0.08	0.30	0.28
Tracheal	0.60	<b>0.02</b>	0.68	<b>0.01</b>	0.78	<b>&lt;0.01</b>	0.52	<b>0.05</b>	0.50	0.06	0.55	<b>0.03</b>	0.33	0.23
Anterior	0.75	<b>&lt;0.01</b>	0.81	<b>&lt;0.01</b>	0.80	<b>&lt;0.01</b>	0.76	<b>&lt;0.01</b>	0.63	<b>0.01</b>	0.59	<b>0.02</b>	0.68	<b>&lt;0.01</b>

Note: Correlation coefficients calculated for Center 1 and Center 2 combined. Significant *p*-values are printed in bold.

Abbreviations: DCE, dynamic contrast-enhanced; QDP, perfusion defect percentage; PREFUL, phase-resolved functional lung; ROI, region of interest.



**FIGURE 5** Comparison of spatial overlap between phase-resolved functional lung (PREFUL) and dynamic contrast-enhanced (DCE) perfusion defect percentage (QDP) maps of Center 1 and Center 2 for the whole lung (a) as well as the posterior (b), tracheal (c), and anterior (d) slices. The central red line indicates the median and the bottom and top edges of the box in the 25<sup>th</sup> and 75<sup>th</sup> percentiles. The whiskers extend to the most extreme data points not considering outliers. Data points outside the whiskers are outliers. *p*-values obtained by Wilcoxon rank-sum test.

size was used to reduce the influence of noise on the correlation by averaging the signal of 8 voxels. No or low correlations, especially in the lung periphery, might be explained by inaccurate registration of PREFUL images to DCE images (Figure S3). A much deeper level of inspiration during DCE data acquisition (deep inspiration in breath-hold) when compared to PREFUL MRI (inspiration during tidal breathing) can lead to misalignment around the diaphragm and heart and in the subpleural regions of the lung. Hence, in these regions

slightly different parts of the lung are compared between PREFUL and DCE (Figure S3). In addition, incomplete breath-holds during DCE data acquisition result in residual movement and thus lead to artificially high perfusion values around the diaphragm (Figure S3). As a consequence, misaligned regions after registration as well as regions affected by respiratory motion during DCE acquisition were removed from the segmentation mask. Further, artifacts due to cardiac motion, especially in anterior slices and in the lower left lung, may have

affected image quality. Lower correlations in the anterior slices might also be caused by the smaller size of the segmented lung region.

For a better spatial alignment of PREFUL and DCE images after co-registration, PREFUL images were first registered towards one image at end inspiration. However, the PREFUL registration to inspiration can cause registration artifacts around the diaphragm and a remaining movement of vessels (Movie S1) might lead to inaccurate perfusion values in these regions.

A semiquantitative approach for further perfusion assessment is the generation of binary perfusion defect maps. In accordance with recent single-center studies,<sup>28,29</sup> good spatial agreement was found comparing PREFUL and DCE QDP-maps.

For PREFUL MRI, significant correlations between QDP and FEV1 predicted were found for the whole lung, whereas for DCE MRI the correlation was moderate but not significant. However, correlation coefficients were similar to those obtained by Kaireit et al.<sup>28</sup> The slightly lower correlations and missing significance for DCE may be explained by several reasons including low number of study participants. Further, QDP is a perfusion parameter and FEV1 predicted a ventilation parameter. Therefore, any mismatches between perfusion and ventilation defects could have an influence on the correlation between QDP and FEV1 predicted. Also, in contrast to global lung function measurement of FEV1, both MRI methods included only 5–8 slices in the calculation of the QDP value for the whole lung, which still leaves gaps in a full coverage of the whole lung parenchyma.

Although the correlations of normalized perfusion-weighted values were moderate, good correlation coefficients were found for QDP between PREFUL and DCE for both centers combined. However, some patients showed QDP differences  $> 10\%$  ( $QDP_{DCE} - QDP_{PREFUL}$ ). Differences between QDP values obtained by PREFUL and DCE could be explained by the lower resolution of PREFUL compared to DCE, resulting in partial volume effects of the central pulmonary vessels. This may contribute to imprecise estimation of perfused areas. In addition, for DCE MRI the perfusion signal depends on the local concentration of contrast agent in the tissue and is described by means of contrast agent dynamics, whereas for PREFUL MRI perfusion is given by mapping of the pulmonary arterial pulse wave during the cardiac cycle.<sup>21</sup> As the mechanism of pulmonary blood flow measurement of the two methods is intrinsically different, differences in perfusion-weighted values and hence in QDP values may occur. Further, perfusion-weighted DCE values represent the signal intensity for every voxel at that time when the contrast agent is inside the lung parenchyma. The signal intensity in turn is given by the

amount of contrast agent present in each voxel and the contrast agent transit depends on the tissue perfusion. For PREFUL MRI, perfusion-weighted values represent the signal intensity for every voxel caused by inflowing blood transported by the pulmonary arterial pulse wave at that time when most voxels inside the lung parenchyma reach their maximal signal intensity. Due to the different mechanisms of blood flow measurements for DCE and PREFUL MRI, the selection of the perfusion-weighted phase is different for DCE and PREFUL. The intention for both methods was to select a perfusion phase at which nondefect parenchyma voxels reach their maximal perfusion signal. For DCE MRI, this is related to the phase when the contrast agent starts to reach the aortic arch. Therefore, this timepoint was selected as perfusion-weighted DCE phase. For PREFUL MRI, the assumption was made, that for nondefect parenchyma voxels the pulse wave is not impaired by constricted vessels and that therefore they would reach their maximal signal approximately at the same time. Whereas for defect voxels the pulse wave is impaired, so that these voxels will reach their maximal signal intensity at different timepoints. Hence the phase at which most voxels reach their maximal signal intensity was selected as perfusion-weighted PREFUL phase.

A prerequisite to calculate QDP maps is the definition of the threshold to define nondefect parenchyma. Especially voxels with signal values close to the threshold could be considered as perfusion defect/nondefect by just one method (PREFUL or DCE) and hence contribute to differences in QDP values. Various threshold approaches such as linear binning,<sup>38,39,40</sup> percentile, and median of lung parenchyma values<sup>28,29,37</sup> or a specific percentage of the highest value<sup>41,42</sup> were presented and validated in recent studies for different imaging techniques. Therefore, to determine a best possible threshold for QDP calculation, a threshold analysis before the actual study to assess these methods for PREFUL and DCE MRI was performed. A more detailed discussion of the threshold analysis can be found in the appendix.

Moreover, artifacts due to cardiac motion may also explain QDP differences between PREFUL and DCE.

No significant difference between median QDP values derived by PREFUL and DCE was found for Center 1 as well as for Center 2 and, in accordance with the spirometry outcomes, Center 2 showed higher median QDP values compared to Center 1.

Comparing the spatial overlap between PREFUL and DCE QDP maps derived for both centers separately, overlap values, found for the three central slices, were not significantly different for Center 1 and Center 2. However, Center 1 showed significantly higher spatial overlap values for the whole lung compared to Center 2.

This might be explained by the increased severity of lung disease seen in patients from Center 2 when compared to Center 1 as reflected in the lower spirometry outcomes and higher QDP values. Given the lower QDP values seen in the group of patients analyzed from Center 1 when compared to Center 2, it would be expected that the impact of mismatching perfusion defect/nondefect areas between PREFUL and DCE to the overall spatial overlap is much smaller for patients of Center 1 compared to Center 2. Moreover, there was a higher difference between PREFUL and DCE QDP values for Center 2 compared to Center 1, which could also be explained by the more advanced lung disease in patients from Center 2. For these patients, more voxels with perfusion values in the range of the QDP thresholds are expected, which could be counted as perfusion defect for PREFUL but not for DCE or vice versa. As a result, this could have led to an inferior spatial overlap for Center 2.

## LIMITATIONS

One limitation of this study is that data acquisition was performed with slightly different temporal and spatial resolution across centers and imaging methods. Therefore, depending on the resolution, widening and blurring of vessels as well as partial volume effects are differently manifested, affecting the calculated perfusion-weighted maps and hence the QDP maps. Further, the temporal resolution has an impact on the interpolation process during PREFUL phase sorting, which might affect the consistency of the selected cardiac phase for perfusion analysis. Additionally, for DCE MRI, higher temporal resolution led to improved tracking of the contrast bolus pass through the lung parenchyma, since more time points are acquired, enabling a more precise determination of the optimal perfusion-weighted DCE phase, although this may not be the same perfusion phase as derived from PREFUL analysis, leading to differences in perfusion maps.

Moreover, DCE MRI is a 3D technique capable of imaging the whole lung, whereas for PREFUL MRI an incomplete coverage of the lung is performed with multiple 2D slices. Since for PREFUL MRI the inflow of nonexcited blood during every RF pulse excitation is essential for generating perfusion signal, a slice selective excitation is necessary and therefore a 3D technique as used for DCE MRI is not feasible. Finally, only a small number of patients from each site, with a smaller number for Center 2, were evaluated in this study. Therefore, a more detailed assessment of the quality of PREFUL MRI compared to DCE MRI is difficult. However, this study permits a first comparison of

PREFUL MRI across different centers and scanners, which serves as a starting point for future multicenter studies.

Despite those limitations, since PREFUL MRI is a contrast agent-free imaging technique performed in free-breathing, it could be used as a pulmonary perfusion assessment tool in patients who cannot or should not receive contrast agents or ionizing radiation such as pregnant women or children. In addition, PREFUL MRI can be used for monitoring pulmonary perfusion in patients with chronic lung disease who need regular lung surveillance.

## CONCLUSION

In conclusion, similar results were observed with perfusion-weighted PREFUL MRI in comparison with DCE MRI in this dual center, dual vendor study. This is an important step towards clinical implementation of noncontrast-enhanced lung perfusion methods such as PREFUL MRI.

## AUTHOR CONTRIBUTIONS

*Study design:* Lea Behrendt, Jim M. Wild, Jens Vogel-Claussen. *Data collection:* Laurie J. Smith, Andreas Voskrebenev, Filip Klimeš, Anna-Maria Dittrich, Helen Marshall. *Data analysis:* Lea Behrendt, Andreas Voskrebenev, Filip Klimeš. *Study supervision:* Lea Behrendt, Helen Marshall, Jim M. Wild, Jens Vogel-Claussen. *Manuscript writing:* Lea Behrendt. *Critical revisions for important intellectual content:* Lea Behrendt, Laurie J. Smith, Andreas Voskrebenev, Filip Klimeš, Till F. Kaireit, Gesa H. Pöhler, Agilo L. Kern, Cristian Crisosto Gonzalez, Anna-Maria Dittrich, Helen Marshall, Katharina Schütz, Paul J. C. Hughes, Pierluigi Ciet, Harm A. W. M. Tiddens, Jim M. Wild, Jens Vogel-Claussen.

## ACKNOWLEDGMENTS

The authors would like to thank Melanie Pfeifer, Frank Schröder, Lars Kähler, and all involved radiographers for outstanding technical assistance in performing the MRI measurements as well as all patients for attending. The authors disclosed receipt of the following financial support for the research, authorship, and/or publication of this article. The work was funded by the German Center for Lung Research (DZL) and by the Cystic Fibrosis Foundation (CFF) (grant number TIDDE-N17A0). The funders had no role in study design, data collection and analysis, decision to publish, or preparation of the manuscript. Open Access funding enabled and organized by Projekt DEAL.

## CONFLICTS OF INTEREST

The authors declare no conflicts of interest.

## ETHICS STATEMENT

This study was approved by the local Ethics Committees and written informed consent was obtained from all patients.

## ORCID

Lea Behrendt  <http://orcid.org/0000-0001-8851-1849>

Agilo L. Kern  <http://orcid.org/0000-0003-4157-9808>

## REFERENCES

- Mall MA, Hartl D. CFTR: cystic fibrosis and beyond. *Eur Respir J*. 2014;44:1042–54.
- Elborn JS. Cystic fibrosis. *The Lancet*. 2016;388:2519–31.
- Dodge JA, Lewis PA, Stanton M, Wilsher J. Cystic fibrosis mortality and survival in the UK: 1947–2003. *Eur Respir J*. 2007;29:522–6.
- Sommerburg O, Hammermann J, Lindner M, Stahl M, Muckenthaler M, Kohlmüller D, Happich M, Kulozik AE, Stopsack M, Gahr M, Hoffmann GF, Mall MA. Five years of experience with biochemical cystic fibrosis newborn screening based on IRT/PAP in Germany. *Pediatr Pulmonol*. 2015;50:655–64.
- Ratjen F, Bell SC, Rowe SM, Goss CH, Quittner AL, Bush A. Cystic fibrosis. *Nat Rev Dis Primers*. 2015;1:15010.
- Hurley MN, McKeever TM, Prayle AP, Fogarty AW, Smyth AR. Rate of improvement of CF life expectancy exceeds that of general population—observational death registration study. *J Cyst Fibros*. 2014;13:410–5.
- Kołodziej M, de Veer MJ, Cholewa M, Egan GF, Thompson BR. Lung function imaging methods in cystic fibrosis pulmonary disease. *Respir Res*. 2017;18:773. <https://doi.org/10.1186/s12931-017-0578-x>
- O'Connell OJ, McWilliams S, McGarrigle A, O'Connor OJ, Shanahan F, Mullane D, Eustace J, Maher MM, Plant BJ. Radiologic imaging in cystic fibrosis: cumulative effective dose and changing trends over 2 decades. *Chest*. 2012;141:1575–83.
- Kuo W, Ciet P, Tiddens HA, Zhang W, Guillerman RP, van Straten M. Monitoring cystic fibrosis lung disease by computed tomography: radiation risk in perspective. *Am J Respir Crit Care Med*. 2014;189:1328–36.
- Johns CS. Lung perfusion: MRI vs. SPECT for screening in suspected chronic thromboembolic pulmonary hypertension. *J Magn Reson Imaging*. 2017;46:1693–7.
- Rajaram S, Swift AJ, Telfer A, Hurdman J, Marshall H, Lorenz E, Capener D, Davies C, Hill C, Elliot C, Condliffe R, Wild JM, Kiely DG. 3D contrast-enhanced lung perfusion MRI is an effective screening tool for chronic thromboembolic pulmonary hypertension: results from the ASPIRE Registry. *Thorax*. 2013;68:677–8.
- Ingrisch M, Maxien D, Schwab F, Reiser MF, Nikolaou K, Dietrich O. Assessment of pulmonary perfusion with breath-hold and free-breathing dynamic contrast-enhanced magnetic resonance imaging. *Invest Radiol*. 2014;49:382–9.
- Chen L, Liu D, Zhang J, Xie B, Zhou X, Grimm R, Huang X, Wang J, Feng L. Free-breathing dynamic contrast-enhanced MRI for assessment of pulmonary lesions using golden-angle radial sparse parallel imaging. *J Magn Reson Imaging*. 2018;48:459–68.
- Kanda T, Ishii K, Kawaguchi H, Kitajima K, Takenaka D. High signal intensity in the dentate nucleus and globus pallidus on unenhanced T1-weighted MR images: relationship with increasing cumulative dose of a gadolinium-based contrast material. *Radiology*. 2014;270:834–41.
- Gulani V, Calamante F, Shellock FG, Kanal E, Reeder SB. Gadolinium deposition in the brain: summary of evidence and recommendations. *The Lancet Neurology*. 2017;16:564–70.
- Choi JW, Moon WJ. Gadolinium deposition in the brain: current updates. *Korean J Radiol*. 2019;20:134–47.
- Kanal E. Gadolinium based contrast agents (GBCA): safety overview after 3 decades of clinical experience. *Magn Reson Imaging*. 2016;34:1341–5.
- Stanescu AL, Shaw DW, Murata N, Murata K, Rutledge JC, Maloney E, Maravilla KR. Brain tissue gadolinium retention in pediatric patients after contrast-enhanced magnetic resonance exams: pathological confirmation. *Pediatr Radiol*. 2020;50:388–96.
- Bauman G, Puderbach M, Deimling M, Jellus V, Chef'd'hotel C, Dinkel J, Hintze C, Kauczor HU, Schad LR. Non-contrast-enhanced perfusion and ventilation assessment of the human lung by means of Fourier decomposition in proton MRI. *Magn Reson Med*. 2009;62:656–64.
- Vogel-Claussen J, Schonfeld CO, Kaireit TF, Voskrebenev A, Czerner CP, Renne J, Tillmann HC, Berschneider K, Hiltl S, Bauersachs J, Welte T, Hohlfeld JM. Effect of indacaterol/glycopyrronium on pulmonary perfusion and ventilation in hyperinflated patients with chronic obstructive pulmonary disease (CLAIM) a double-blind, randomized, crossover trial. *Am J Respir Crit Care Med*. 2019;199:1086–96.
- Pohler GH, Klimes F, Voskrebenev A, Behrendt L, Czerner C, Gutberlet M, Cebotari S, Ius F, Fegbeutel C, Schoenfeld C, Kaireit TF, Hauck EF, Olsson KM, Hoepfer MM, Wacker F, Vogel-Claussen J. Chronic thromboembolic pulmonary hypertension perioperative monitoring using phase-resolved functional lung (PREFUL)-MRI. *J Magn Reson Imaging*. 2020;52:610–9.
- Voskrebenev A, Gutberlet M, Klimes F, Kaireit TF, Schonfeld C, Rotarmel A, Wacker F, Vogel-Claussen J. Feasibility of quantitative regional ventilation and perfusion mapping with phase-resolved functional lung (PREFUL) MRI in healthy volunteers and COPD, CTEPH, and CF patients. *Magn Reson Med*. 2018;79:2306–14.
- Glandorf J, Klimes F, Voskrebenev A, Gutberlet M, Behrendt L, Crisosto C, Wacker F, Ciet P, Wild JM, Vogel-Claussen J, Baltzer PAT. Comparison of phase-resolved functional lung (PREFUL) MRI derived perfusion and ventilation parameters at 1.5T and 3T in healthy volunteers. *PLoS One*. 2020;15:e0244638.
- Klimes F, Voskrebenev A, Gutberlet M, Kern AL, Behrendt L, Grimm R, Suhling H, Crisosto CG, Kaireit TF, Pohler GH, Glandorf J, Wacker F, Vogel-Claussen J. 3D phase-resolved functional lung ventilation MR imaging in healthy volunteers and patients with chronic pulmonary disease. *Magn Reson Med*. 2021;85:912–25.
- Pöhler GH, Klimeš F, Behrendt L, Voskrebenev A, Gonzalez CC, Wacker F, Hohlfeld JM, Vogel-Claussen J.

- Repeatability of phase-resolved functional lung (PREFUL)-MRI ventilation and perfusion parameters in healthy subjects and COPD Patients. *J Magn Reson Imaging*. 2020;53:915–27. <https://doi.org/10.1002/jmri.27385>
26. Munidasa S, Couch MJ, Rayment JH, Voskrebenev A, Seethamraju R, Vogel-Claussen J, Ratjen F, Santyr G. Free-breathing MRI for monitoring ventilation changes following antibiotic treatment of pulmonary exacerbations in paediatric cystic fibrosis. *Eur Respir J*. 2021;57:2003104. <https://doi.org/10.1183/13993003.03104-2020>
  27. Couch MJ, Munidasa S, Rayment JH, Voskrebenev A, Seethamraju RT, Vogel-Claussen J, Ratjen F, Santyr G. Comparison of functional free-breathing pulmonary 1H and hyperpolarized 129Xe magnetic resonance imaging in pediatric cystic fibrosis. *Acad Radiol*. 2020;28:e209–18. <https://doi.org/10.1016/j.acra.2020.05.008>
  28. Kaireit TF. Comparison of quantitative regional perfusion-weighted phase resolved functional lung (PREFUL) MRI with dynamic gadolinium-enhanced regional pulmonary perfusion MRI in COPD patients. *J Magn Reson Imaging*. 2019;49:1122–32.
  29. Behrendt L, Voskrebenev A, Klimes F, Gutberlet M, Winther HB, Kaireit TF, Alsady TM, Pohler GH, Derlin T, Wacker F, Vogel-Claussen J. Validation of automated perfusion-weighted phase-resolved functional lung (PREFUL)-MRI in patients with pulmonary diseases. *J Magn Reson Imaging*. 2020;52:103–14.
  30. Griswold MA, Jakob PM, Heidemann RM, Nittka M, Jellus V, Wang J, Kiefer B, Haase A. Generalized autocalibrating partially parallel acquisitions (GRAPPA). *Magn Reson Med*. 2002;47:1202–10.
  31. Voskrebenev A, Gutberlet M, Kaireit TF, Wacker F, Vogel-Claussen J. Low-pass imaging of dynamic acquisitions (LIDA) with a group-oriented registration (GOREG) for proton MR imaging of lung ventilation. *Magn Reson Med*. 2017;78:1496–1505.
  32. Avants BB, Tustison NJ, Song G, Cook PA, Klein A, Gee JC. A reproducible evaluation of ANTs similarity metric performance in brain image registration. *Neuroimage*. 2011;54:2033–44.
  33. Simonyan K, Zisserman A. Very deep convolutional networks for large-scale image recognition. 3rd International Conference on Learning Representations, ICLR 2015—Conference Track Proceedings. International Conference on Learning Representations, ICLR. 2015.
  34. Otsu N. Threshold selection method from gray-level histograms. *IEEE Trans Syst Man Cybern*. 1979;SMC-9:62–6.
  35. Masy M, Giordano J, Petyt G, Hossein-Foucher C, Duhamel A, Kyheng M, De Groote P, Fertin M, Lamblin N, Bervar JF, Remy J, Remy-Jardin M. Dual-energy CT (DECT) lung perfusion in pulmonary hypertension: concordance rate with V/Q scintigraphy in diagnosing chronic thromboembolic pulmonary hypertension (CTEPH). *Eur Radiol*. 2018;28:5100–10.
  36. Hopkins SR, Wielpütz MO, Kauczor HU. Imaging lung perfusion. *J Appl Physiol*. 2012;113:328–39.
  37. Bauman G, Puderbach M, Heimann T, Kopp-Schneider A, Fritzsche E, Mall MA, Eichinger M. Validation of Fourier decomposition MRI with dynamic contrast-enhanced MRI using visual and automated scoring of pulmonary perfusion in young cystic fibrosis patients. *Eur J Radiol*. 2013;82:2371–7.
  38. He M, Kaushik SS, Robertson SH, Freeman MS, Virgincar RS, McAdams HP, Driehuys B. Extending semiautomatic ventilation defect analysis for hyperpolarized 129Xe ventilation MRI. *Acad Radiol*. 2014;21:1530–41.
  39. He M, Driehuys B, Que LG, Huang YCT. Using Hyperpolarized 129Xe MRI to quantify the pulmonary ventilation distribution. *Acad Radiol*. 2016;23:1521–31.
  40. He M, Wang Z, Rankine L, Luo S, Nouis J, Virgincar R, Mamarappallil J, Driehuys B. Generalized linear binning to compare hyperpolarized 129Xe ventilation maps derived from 3D radial gas exchange versus dedicated multislice gradient echo MRI. *Acad Radiol*. 2020;27:e193–203.
  41. Derlin T, Kelting C, Hueper K, Weiberg D, Meyer K, Olsson KM, Thackeray JT, Welte T, Bengel FM, Hoepfer MM. Quantitation of perfused lung volume using hybrid SPECT/CT allows refining the assessment of lung perfusion and estimating disease extent in chronic thromboembolic pulmonary hypertension. *Clin Nucl Med*. 2018;43:e170–7.
  42. Schmuck S, Von Klot CA, Henkenberens C, Sohns JM, Christiansen H, Wester HJ, Ross TL, Bengel FM, Derlin T. Initial experience with volumetric 68Ga-PSMA I&T PET/CT for assessment of whole-body tumor burden as a quantitative imaging biomarker in patients with prostate cancer. *J Nucl Med*. 2017;58:1962–8.

## SUPPORTING INFORMATION

Additional supporting information can be found online in the Supporting Information section at the end of this article.

**How to cite this article:** Behrendt L, Smith LJ, Voskrebenev A, Klimes F, Kaireit TF, Pöhler GH, Kern AL, Gonzalez CC, Dittrich AM, Marshall H, Schütz K, Hughes PJC, Ciet P, Tiddens HAWM, Wild JM, Vogel-Claussen J. A dual center and dual vendor comparison study of automated perfusion-weighted phase-resolved functional lung magnetic resonance imaging with dynamic contrast-enhanced magnetic resonance imaging in patients with cystic fibrosis. *Pulm Circ*. 2022;12:e12054. <https://doi.org/10.1002/pul2.12054>